Experimental Realization of a Passive Gigahertz Frequency-Division Demultiplexer for Magnonic Logic Networks

Frank Heussner,* Giacomo Talmelli, Moritz Geilen, Björn Heinz, Thomas Brächer, Thomas Meyer, Florin Ciubotaru, Christoph Adelmann, Kei Yamamoto, Alexander A. Serga, Burkard Hillebrands, and Philipp Pirro

The emerging field of magnonics uses spin waves and their quanta, magnons, to implement wave-based computing on the micro- and nanoscale. Multifrequency magnon networks would allow for parallel data processing within single logic elements, whereas this is not the case with conventional transistor-based electronic logic. However, a lack of experimentally proven solutions to efficiently combine and separate magnons of different frequencies has impeded the intensive use of this concept. Herein, the experimental realization of a spin-wave demultiplexer enabling frequency-dependent separation of magnonic signals in the gigahertz range is demonstrated. The device is based on 2D magnon transport in the form of spin-wave beams in unpatterned magnetic films. The intrinsic frequency dependence of the beam direction is exploited to realize a passive functioning obviating an external control and additional power consumption. This approach paves the way to magnonic multiplexing circuits enabling simultaneous information transport and processing.

The concept of parallel data processing in single elements is very promising as it can multiply the throughput of future logic networks significantly.[1] One important requirement, the wave-based processing of data, has already been demonstrated using spin waves[2] in micro- and nanostructures.[3,4] Furthermore, the similar necessary technique of simultaneous information transport in separated frequency-channels, called frequency-division multiplexing,[5] has been used in various other wave-based applications such as in fiber-optic networks. However, its implementation into magnonic networks has only been studied theoretically[1,6] or discussed in preparatory

works,[7–9] as a device for the efficient combination and separation of spin-wave signals of different frequencies is missing until now. In this work, we present the experimental realization of this required device, which uses caustic-like spin-wave beams to create a so-called magnonic frequency-division demultiplexer. Hence, our results enable the realization of magnonic multifrequency circuits[6] which allow for parallel data processing in single devices.[1]

Spin waves offer many advantages for wave-based computing[10–15] due to their micro- to nanometer small wavelengths at gigahertz frequencies,[16–18] their enormous tunability by various parameters[19] and the possibility of chargeless information transport. One exceptional property utilized in the following work is the anisotropic propagation of spin waves in suitable magnetic media, which can lead to the creation of narrow spin-wave beams and caustics[6,20–27] (see Experimental Section). Their subwavelength transverse aperture[24] is an outstanding reason for their potential use in nanostructured networks, especially when considering the beam formation of high-wavevector magnons.[21] The caustic-like spin-wave beams can be radiated from point-like sources into unpatterned magnetic films,[22–25] and they are formed due to the noncollinearity of the wavevector and the group velocity vector. Furthermore, their propagation direction can be versatilely controlled by, e.g., frequency,[6,20,22,25–27]

Dr. F. Heussner, M. Geilen, B. Heinz, Dr. T. Brächer, Dr. T. Meyer,[+]
Dr. A. A. Serga, Prof. B. Hillebrands, Prof. P. Pirro
Fachbereich Physik and Landesforschungszentrum OPTIMAS
Technische Universität Kaiserslautern
Kaiserslautern D-67663, Germany
E-mail: heussner@rhrk.uni-kl.de

The ORCID identification number(s) for the author(s) of this article can be found under https://doi.org/10.1002/pssr.201900695.

[+]Present address: THATec Innovation GmbH, Mannheim 68165, Germany

G. Talmelli, Dr. F. Ciubotaru, Dr. C. Adelmann
Imec
Leuven 3001, Belgium

G. Talmelli
Departement Materiaalkunde
SIEM
KU Leuven
Leuven 3001, Belgium

B. Heinz
Graduate School Materials Science in Mainz
Staudingerweg 9, Mainz 55128, Germany

Dr. K. Yamamoto
Advanced Science Research Center
Japan Atomic Energy Agency
Tokai 319-1195, Japan

magnetic field strength,[20] and direction of the local magnetization.[23,24]

In this work, we experimentally demonstrate how these caustic-like spin-wave beams can be used to realize controllable information transport in 2D magnetic films with thicknesses of a few tens of nanometers. The guidance is neither achieved by geometrical structuring[2,3] nor by different internal magnetic fields as it has been demonstrated, e.g., in bicomponent magnonic crystals which offer different spatial channels for different spin-wave frequencies.[28,29] Our system is also not relying on inhomogeneous magnetic ground states,[30] but it guides the waves purely by the anisotropy of the magnonic system. Utilizing this anisotropic signal propagation allows for the realization of passive elements without any additional energy consumption as the magnonic system inherently collimates and steers the energy transport. As just one of the many possible applications of this concept, we present the realization of a passive demultiplexer exploiting the frequency dependence of the beam direction. By inverting the geometry, i.e., inverting the role of the input and output waveguides, a multiplexer can be realized equally well.[31]

The experimental realization of the frequency-division demultiplexer is based on a 30 nm-thin film of the magnetic alloy CoFeB. In contrast to magnetic insulators like yttrium iron garnet (YIG),[26] the metallic ferromagnet CoFeB is much more compatible with state-of-the-art fabrication techniques of silicon-based microchips. Furthermore, CoFeB exhibits a much higher saturation magnetization (see Experimental Section), which enables the creation of caustic-like spin-wave beams in a broad-frequency range. Based on our previous studies,[6] we have designed a demultiplexer prototype by micromagnetic modeling. Subsequently, the sample has been fabricated and studied by detecting the spin-wave intensity using micro-focused Brillouin light-scattering spectroscopy (μBLS).[32] After investigating the frequency dependence of the spin-wave beam directions and comparing it with theoretical calculations, we verify the full functionality of the demultiplexer by 2D measurements of the spin-wave intensity.

Figure 1a,b shows the simulated intensity distribution inside of the designed structure for spin waves of frequencies $f_1 = 11.2$ GHz and $f_2 = 13.8$ GHz. The dashed arrows mark the beam directions that are predicted by the developed theoretical model (see Figure 1c and Experimental Section). The functional part of the device comprises the unpatterned area in the center of the structure in which the 2D energy transport takes place. Input and output waveguides, which can serve as interfaces to adjacent magnonic building blocks in larger magnonic networks, are connected to this area. To provide an input signal, magnon excitation is simulated by applying localized alternating magnetic fields h_{rf} inside the input waveguide. The field distribution is chosen in accordance with the experiment in which these fields are created by microwave currents flowing through a microstrip antenna placed across the waveguide. The spin waves propagate toward the unpatterned area and, in agreement with previous observations,[6,22–24] two symmetric spin-wave beams are emitted from the waveguide opening, which acts as a point-like source exhibiting a broad wavevector spectrum. The anisotropy of the spin-wave dispersion leads to a strong focusing of the energy. Furthermore, the initial width of the
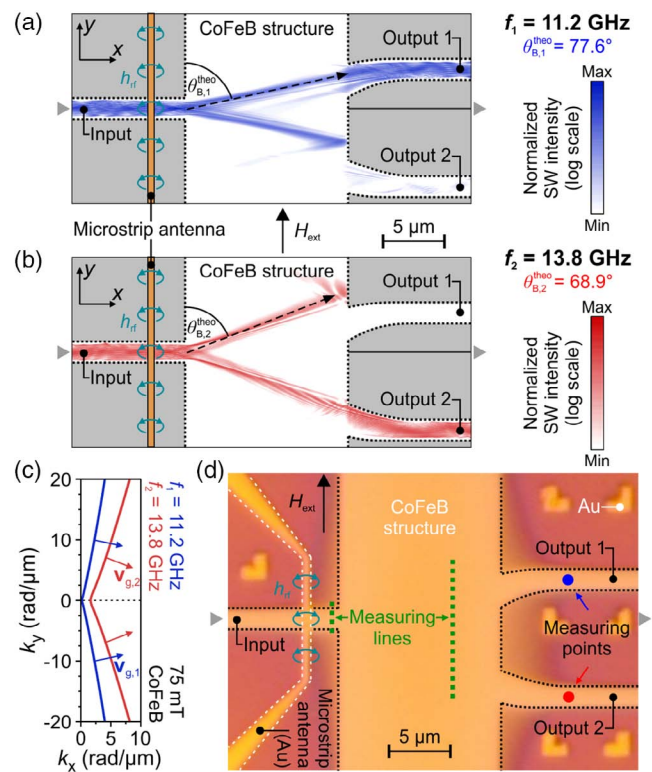

Figure 1. Micromagnetic modeling of the frequency-division demultiplexer and microscope image of the fabricated sample. The positions of the output waveguides along the y-direction are asymmetric with respect to the input waveguide which enables the demultiplexing functionality of the device. a) Design of the demultiplexer and simulated spin-wave propagation at $f_1 = 11.2$ GHz. The signal is guided from the input waveguide into output 1 by a spin-wave beam. b) Spin-wave distribution at $f_2 = 13.8$ GHz. The signal is channeled into output 2 due to the changed direction of the spin-wave beams in the unstructured film area. c) Isofrequency curves of the studied system. The directions of the group velocity vectors, which are perpendicular to the curve, vary with spin-wave carrier frequency. d) Fabricated sample according to the developed layout of the demultiplexer.

spin-wave beams is determined by the width of the waveguide opening, for which reason an abrupt transition into the unstructured film area without widening was chosen. The observed frequency dependence of the beam directions is utilized to realize the demultiplexing functionality by properly adding two output waveguides after a certain propagation distance. Their positions are asymmetric with respect to the input, leading to the following consequence: at frequency $f_1 = 11.2$ GHz (Figure 1a), the upper spin-wave beam, which propagates at an angle of $\theta_{B,1}^{theo} = 77.6°$ as predicted by the theoretical model, is channeled into output 1 and transmits the information through the device. The lower one is blocked by the edge of the magnetic structure so that the signal cannot reach output 2. In contrast, the beam angles of spin waves of frequency $f_2 = 13.8$ GHz are changed to $\theta_{B,2}^{theo} = 68.9°$ ($\theta'_{B,2} = 180° - \theta_{B,2}$, respectively) resulting in a sole signal transmission into output 2 (Figure 1b). Hence, the device separates spin-wave signals of two frequencies into two spatially detached output waveguides, whose transition zones

are especially tailored to enable an efficient channeling of the spin waves into the first waveguide mode and to avoid reflections. The exploited frequency dependence of the beam directions results from the modification of the spin-wave isofrequency curve with frequency (see Figure 1c) and the according variation of the group-velocity vectors, which are always perpendicular to this curve (see Experimental Section). It should be mentioned that the exact operating frequencies of the device can be controlled by changing, e.g., the external field strength since this shifts the magnon dispersion. Here, the external magnetic field is set to $\mu_0 H_{ext} = 75\,mT$.

Based on the design developed and optimized by micromagnetic modeling, the prototype of the passive demultiplexer has been fabricated based on a 30 nm-thin film of CoFeB, as shown in Figure 1d. To prove the functionality of the frequency-division demultiplexer, μBLS measurements of the spin-wave intensity have been performed at two positions in the center of the output waveguides, as shown in Figure 1d. Spin waves are excited in the input in a frequency range from 10.5 to 15.5 GHz in the steps of 0.1 GHz by applying an according microwave signal to the microstrip antenna. **Figure 2**a shows the detected frequency dependence of the spin-wave intensity in the two spatially detached output waveguides. A clear separation of spin-wave signals depending on their frequency is visible. Signals in the narrow range from 10.8 to 11.8 GHz are channeled into output 1. In contrast, output 2 accepts only spin waves in the broader frequency band from 12.3 to 15.3 GHz, hence, without any overlap. This measurement clearly demonstrates that spin-wave signals with appropriately chosen frequencies, e.g., the frequencies of maximum intensity in the different outputs $f_1 = 11.2\,GHz$ and $f_2 = 13.8\,GHz$, are spatially separated by the prototype device as predicted by the micromagnetic modeling.

The beam angle θ_B shown in Figure 2b is experimentally determined by measuring the spin-wave intensity along a line in the input transition zone (left green dotted line, Figure 1d) and along a line in the second third of the unpatterned area (right green dotted line, Figure 1d). From the observed shift of the intensity maxima, the angle θ_B is calculated. No beams are detected below 10.8 GHz as the dispersion relation is very flat until the frequency of ferromagnetic resonance $f_{FMR} = 10.94\,GHz$ is reached. The measured data agrees well with the theoretically predicted curve (solid line in Figure 2b). This is due to the fact that, in addition to the peculiarities of anisotropic magnon propagation,[20] our model considers such important parameters like the excited wavevector spectrum and the distance between the observation point and the source. The optimum angles $\theta_{B,1}^{exp} = 77.9°$ and $\theta_{B,2}^{exp} = 69.6°$, leading to maximum intensity in the outputs, are shown in Figure 2b together with the shaded acceptance intervals, which result from the assumption that beams are channeled into the outputs if their direction deviates less than 2.5° from the optimum angles. These acceptance intervals in combination with the curve $\theta_B(f)$ can explain the differing widths of the accepted frequency bands of the two outputs: The angle variation is quite large in the region of $f_1 = 11.2\,GHz$. Hence, only frequencies within a small range around f_1 create beams whose directions lie inside the angular acceptance interval of output 1. In contrast, the slope of the mentioned curve is significantly lower at $f_2 = 13.8\,GHz$. Thus, a larger variation of the
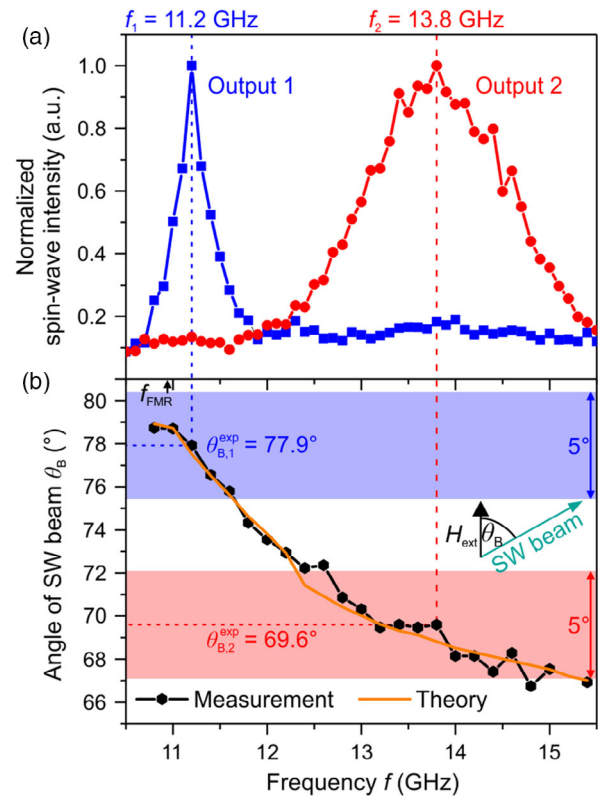

Figure 2. Experimental realization of spin-wave demultiplexing using the developed prototype device. a) Frequency-dependence of the spin-wave intensity in the output waveguides measured by μBLS. Spin-wave signals are detected inside the two outputs within nonoverlapping frequency ranges exhibiting signal maxima at the frequencies f_1 and f_2. b) The measured frequency-dependence of the direction of the spin-wave beams is compared with the developed theoretical model. Shaded areas mark the angular intervals of signal acceptance of both outputs. The centers of the intervals are given by the optimal angles $\theta_{B,1}^{exp}$ and $\theta_{B,2}^{exp}$.

frequency is permitted around f_2 until the occurring beam angles are out of the acceptance interval of output 2.

For a detailed visualization, the spin-wave intensity was measured in the entire demultiplexer area at the frequencies f_1 and f_2 by performing 2D μBLS scans. (The experimental proof of the simultaneous transmission of spin waves of these two frequencies through a shared waveguide can be found in the Supporting Information.) A comparison of the 2D measurements (**Figure 3**) with the results of the micromagnetic modeling (Figure 1a,b) reveals a remarkably good agreement. This confirms that the whole demultiplexing mechanism works exactly as predicted and is based on the creation of spin-wave beams, their frequency-dependent propagation though the unstructured area, and the channeling of the signals into different outputs.

Furthermore, these measurements can be used to determine the input–output ratio κ of the device to reveal the influence of the beam formation on signal losses. Considering the transmission from the input waveguide into output 1 at frequency f_1 yields a value of $\kappa_1^{exp} = (-18.1 \pm 2.1)\,dB$, whereas a ratio of $\kappa_2^{exp} = (-18.2 \pm 1.9)\,dB$ is obtained for a signal at frequency f_2 channeled into output 2. For comparison, the ratio κ^{theo}
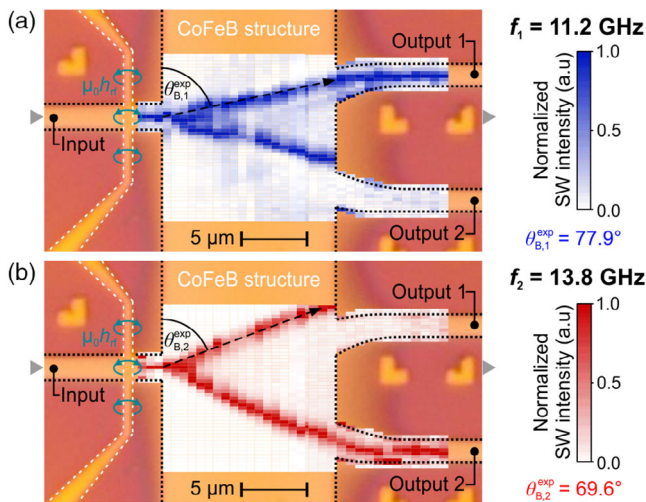
Figure 3. Experimental verification of the beam-based demultiplexing mechanism. µBLS measurements of the spin-wave intensity are performed to visualize the 2D spin-wave transport. The separation of spin-wave signals from one shared input waveguide by frequency-dependent channeling into spatially detached output waveguides occurs due to the intrinsically controlled beam formation. a) Spin-wave guidance into output 1 at $f_1 = 11.2$ GHz and b) into output 2 at $f_2 = 13.8$ GHz.

can be calculated analytically considering the energy splitting and the propagation losses only (see Experimental Section). The resulting values, $\kappa_1^{theo} = (-18.95 \pm 1.84)$ dB and $\kappa_2^{theo} = (-17.64 \pm 1.69)$ dB, show that the major fraction of the losses arise from the intrinsic spin-wave damping during their propagation and not due to the demultiplexing mechanism based on beam formation and channeling (the splitting is suppressible[6]).

Finally, the scalability and advantages of the presented concept should be discussed. The used spin-wave beams are created due to the anisotropy of the magnonic system and, for limited length scales, their width is primary determined by the size of the source.[24] In the presented case, the anisotropy is induced by the dipole–dipole interaction, which is dominant in the low-wavevector range of the magnon spectrum. However, a beam formation is also possible for high-wavevector spin waves whose dispersion characteristics are mainly dominated by the exchange interaction.[21] Hence, the presented concept to guide 2D energy transport by spin-wave beams, formed due to the intrinsic anisotropy of the system, can be scaled down to significantly smaller length scales. Furthermore, the passive character of the signal steering is an important advantage over other concepts requiring energy-consuming external control. This is the case, e.g., with the previously demonstrated spin-wave time-division multiplexer, which relies on external charge currents.[33]

In conclusion, we have developed and experimentally realized a passive frequency-division demultiplexer, which is based on intrinsically steered 2D signal transport in unpatterned magnetic films. The prototype device enables the spatial separation of spin-wave signals of different frequencies. It exploits the frequency-dependence of the direction of narrow spin-wave beams, which are formed in in-plane magnetized films due to the anisotropic spin-wave dispersion. A theoretical approach to predict the beam directions has been developed and verified. The utilized beam

steering requires no external control or additional power consumption, and it can be used to realize a whole multifrequency circuit which enables simultaneous data transport through single transmission lines using the technique of frequency-division multiplexing. This is the basis for exploiting one of the main advantages of wave-based computing, namely, the technique of parallel data processing in single devices, which can now be implemented in an energy-efficient way building on the presented prototype.

Experimental Section

µBLS Measurements: The spin-wave intensity was experimentally measured using µBLS[32] with a spatial resolution of around 250 nm. In all cases, the shown spin-wave intensity of frequency f is the detected time-averaged µBLS intensity integrated over the frequency interval $[f - 0.25$ GHz, $f + 0.25$ GHz$]$. The error of the measured beam angles θ_B shown in Figure 2b results from the spatial resolution of the setup and is calculated to $3.5°$. For reasons of clarity, error bars are omitted in the figure. The spin-wave intensity shown in Figure 3 is normalized along the y-direction to the interval [0,1] to compensate for the background noise of the setup and for the spin-wave damping so that a clear comparison of the two output signals is easily possible. Due to this normalization, the visibility of spin-wave beams, which are reflected from the edge of the structure and are much weaker than the incident beams, is reduced.

Micromagnetic Modeling: The micromagnetic modeling was conducted using the graphics processing unit-accelerated simulation program MuMax3.[34] The simulated structure of size 31.5 µm $\times 15$ µm $\times 30$ nm was discretized into cells of ≈ 15 nm $\times 15$ nm $\times 30$ nm, leading to a consideration of in-plane wavevectors of at least up to 100 rad µm^{-1}. Furthermore, the experimentally determined material parameters of CoFeB ($M_S = 1558$ kA m^{-1}, $A_{ex} = 17.6$ pJ m^{-1}, $\alpha = 0.0043$) were used. On the outer vertical edges of the waveguides (shape of the structure, as shown in Figure 1), the damping was incrementally increased (25 steps over a distance of 0.5 µm) to a value of $\alpha = 0.5$ to suppress reflections of the spin-wave energy. Furthermore, periodic boundary conditions were used along the horizontal edges of the unstructured film area. Spin-wave excitation and propagation were simulated for 7.5 ns by applying an alternating magnetic field inside the input waveguide. The used field distribution was calculated according to Biot–Savart's law for a 0.5 µm-wide and 100 nm-thick microstrip antenna (as used in the experiment) through which the alternating current (AC) flows (with 5 mA amplitude). The resulting raw data of the modeling were the time-dependent vector of the magnetization inside every cell, which had been saved every 25 ps. A temporal Fourier-transformation of the data from 2.5 to 7.5 ns and a squaring of the resulting amplitude were performed to calculate the frequency-dependent, time-averaged spin-wave intensity. This intensity was integrated over the frequency interval $[f - 0.25$ GHz, $f + 0.25$ GHz$]$, so that a direct comparison with the experimental results obtained by µBLS measurements was possible. Furthermore, the simulated spin-wave intensity distribution shown in Figure 1 is normalized along the y-direction to its sum to compensate for the spin-wave damping and to allow for a clear comparison of the two output signals.

Sample Fabrication: The basis of the sample fabrication[35] was a 30 nm thin film of the magnetic alloy CoFeB, which was deposited as part of the layer stack Ta(3 nm)/CoFeB(30 nm)/Ta(3 nm) onto a Si/SiO$_2$(300 nm) wafer. The film thickness of the magnetic material CoFeB was chosen as a tradeoff so that both an efficient spin-wave beam formation and propagation (rather large film thickness preferred) and an efficient structuring of the device (rather small film thickness preferred) was possible. First, the material parameters of this unpatterned sample were measured using two methods. The saturation magnetization $M_S = 1558$ kA m^{-1} and the Gilbert damping constant $\alpha = 0.0043$ were determined by measurements of the ferromagnetic resonance (FMR). Furthermore, the exchange constant $A_{ex} = 17.6$ pJ m^{-1} resulted from µBLS measurements

**ADVANCED
SCIENCE NEWS**

www.advancedsciencenews.com

pss rrl
physica status solidi

www.pss-rapid.com

of the thermal magnon spectrum and a comparison with analytical calculations according to the theory.[36] Afterward, the magnetic layer was structured by e-beam lithography of a hydrogen silsesquioxane (HSQ) hard mask and subsequent ion beam etching, leaving around 70 nm of the resist on top of the structure. To reduce the height differences, a planarization step using spin-on carbon (SoC) was followed with a subsequent deposition of a 30 nm thin layer of SiN (150 °C, chemical vapor deposition). Finally, the microstrip antenna was fabricated by creating a mask using polymethylmethacrylate (PMMA) resist and e-beam lithography followed by sputtering deposition of Ti (10 nm)/Au (100 nm) and the removal of the unwanted parts by a lift-off process in acetone. The resulting sample is shown in Figure 1d. The magnetic structure consists of an unpatterned film area and three 1.5 μm wide waveguides. The positions of the output waveguides along the y-direction are asymmetric with respect to the input waveguide which enables the demultiplexing functionality of the device, as demonstrated in the main text. The light shading on the edge of the transition zones is due to some residual material, which, however, does not influence the functionality of the device. The 0.5 μm-wide and 100 nm-thick microstrip antenna, which was placed on top of the input waveguide, was connected to a microwave setup consisting of a microwave generator and an amplifier which provided the high-frequency current with a nominal output power of $P = +7$ dBm. The final power reaching the sample was very likely significantly reduced. The rectangular structures around the actual device were used to stabilize the positioning of the μBLS microscope. It should be mentioned that the dimensions of the presented prototype had been chosen to allow for an optical investigation using μBLS. Further miniaturization is possible as discussed in the main text.

Calculation of the Input–Output Ratio κ: To calculate the experimental values κ^{exp} of the input–output ratio, the spin-wave intensity at the position 0.5 μm in front of the input transition zone and the intensity 5.1 μm behind the output transition zone were integrated over the waveguide width and both results were divided by each other. The mentioned error resulted from the deviations around the mean value in case the surrounding measuring points were considered. For both frequencies, the detected intensity inside the output, which was not hit by the spin-wave beam, was equal or only marginally above the noise-level of the μBLS setup. This highlights the pronounced demultiplexing functionality.

The theoretical reference values κ^{theo} were calculated from the distances L which the spin waves had to travel from the position in the input to the position in the output, where the intensity had been measured to determine the experimental value. The calculations were carried out according to the formula

$$\kappa^{theo} = 10\ \log_{10}[1/2\exp(-L_f/(0.5\,\nu_f\,\tau_f) - L_w/(0.5\,\nu_w\,\tau_w))] \tag{1}$$

in which the occurring energy splitting into two spin-wave beams was considered by the factor 1/2. It should be mentioned that the splitting can be suppressed by changing the design of the demultiplexer as shown in the study by Heussner et al.[6] Furthermore, the factor 0.5 had to be introduced as the spin-wave intensity was measured instead of the amplitude.

The group velocity ν of the spin waves differs inside the waveguides (ν_w) and in the unpatterned film area (ν_f) and can be calculated according to the studies by Kalinikos and Slavin and Brächer et al.[36,37] To determine ν_f, the spin-wave wavevector relating to the occurring beam angle was used for the calculations. Furthermore, L_w is the spin-wave propagation distance in the waveguides, whereas L_f is the corresponding distance in the film area. Finally, the spin-wave lifetime τ results from the damping parameter α and was approximated by the value $\tau(k=0)$ at ferromagnetic resonance.[37] For all calculations, the effective values of the magnetic field $\mu_0 H_{eff}$ (75 mT inside the film, 50 mT inside the waveguide) and the waveguide width $w_{eff} = 1.3$ μm were used. These effective values result from the demagnetizing field at the edge of the waveguides and can be extracted from the micromagnetic modeling or calculated as shown in the study by Brächer et al.[37]

The following values were obtained for the different frequencies $f_1 = 11.2$ GHz and $f_2 = 13.8$ GHz: $L_{1,w} = 5.48$ μm, $L_{1,f} = 13.05$ μm,

$\nu_{1,w} = 11.65$ μm ns^{-1}, $\nu_{1,f} = 7.08$ μm ns^{-1}, $\tau_w = 1.284$ ns, $\tau_f = 1.254$ ns, and $L_{2,w} = 5.51$ μm, $L_{2,f} = 13.90$ μm, $\nu_{2,w} = 9.70$ μm ns^{-1}, $\nu_{2,f} = 8.93$ μm ns^{-1} resulting in the values for the input–output ratio κ^{theo} as mentioned in the main text. The error of κ^{theo} was calculated by assuming a slightly larger Gilbert damping parameter ($\alpha = 0.0048$), which was very likely to occur due to, e.g., the structuring process of the device.

Theoretical Description of Spin-Wave Beams and Caustics: The basis of the developed theoretical model is the anisotropic isofrequency curve (Figure 1c), which describes the dependence of the wavevector component k_y on the component k_x at a particular frequency f. The dispersion calculations are based on the study by Kalinikos and Slavin,[36] considering $\mathbf{k}_y \parallel \mathbf{H}_{ext}$, $\mathbf{k}_x \perp \mathbf{H}_{ext}$, $\mu_0 H_{ext} = 75$ mT and the material parameters of CoFeB. The direction of the anisotropic spin-wave propagation can be derived from the curve as the spin-wave group velocity vector is perpendicular to it at every point. For a precise prediction of the resulting spin-wave beam orientation, the excited wavevector spectrum A_k and the distance d between the beam source and the observation point are considered, as explained in the following. This is the main difference to a previous theoretical approach[20] and our results reveal, that the observed direction of maximum focusing is not always given by the caustic direction (according to the study by Veerakumar and Camley,[20] caustics occur at the points of the isofrequency curve where its curvature is zero). Due to this reason, we refer to the observed beams resulting from the focused energy transport as (caustic-like) spin-wave beams instead of caustics.

The first step of the developed approach is to include the wavevector spectrum A_k of the beam source in the calculations. It can be assumed that the spin waves propagate through the input in the form of the first waveguide mode having a sinusoidal shape along the short axis of the waveguide and only one maximum in the center. As soon as the input waves reach the transition zone at the connection between the waveguide and the unstructured area, the waveguide mode acts as a 1D source (with effective width w_{eff}, explanation is given earlier) for secondary spin waves propagating into the unpatterned film area and forming beams due to their anisotropic propagation. The confinement of the mode across the waveguide leads to a broad spectrum A_k of the respective wavevector component k_y, which can be calculated to $A_k(k_y) = \cos(k_y\,w_{eff}/2)/(\pi^2/w_{eff}^2 - k_y^2)$ by spatial Fourier transformation of the mode profile. This spectrum is considered using the following procedure. First, the angle θ_{vg} between the group velocity vector and the external field direction is calculated from the isofrequency curve as a function of the wavevector component k_y. Second, the wavevector spectrum $A_k(k_y)$ is projected onto the curve $\theta_{vg}(k_y)$ by a numerical integration to determine the amount of excited spin waves propagating into the direction θ_{vg}. The result of this procedure is the spin-wave amplitude $A_{SW}^{initial}(\theta_{vg})$, which reflects the angle distribution of the spin-wave flow under consideration of the initial wavevector spectrum A_k. Maxima of $A_{SW}^{initial}(\theta_{vg})$ reveal a wave focusing into the respective directions. Their occurrence can be explained by the fact that the anisotropy of the system leads to isofrequency curves with expanded regions where the group velocity direction θ_{vg} is (nearly) unchanged for a broad range of wavevectors k_y. If the excited spectrum A_k has a significant magnitude in these ranges of k_y, an amplitude concentration occurs into the respective directions θ_{vg} leading to the maxima of $A_{SW}^{initial}(\theta_{vg})$. Hence, these maxima indicate the beam creation.

However, a second step is necessary to precisely determine the beam directions. The beam source described earlier has a certain extent which leads to the fact that the overall spin-wave amplitude at the observation point results from the superposition of spin waves which are generated at different positions within the source. If the observation point is close, the source appears under a large angular range and spin waves from considerably different directions superpose. In this case, the focusing pattern can be significantly influenced. This effect is included in the further calculations by considering both the initial angle distribution of the spin-wave amplitudes $A_{SW}^{initial}(\theta_{vg})$ and the sinusoidal mode profile in the transition zone, which represents the source of the beams. Based on these quantities, the final spin-wave amplitude A_{SW}^{final} at a given observation point is calculated by integrating the amplitudes of all spin waves which originate at different points of the source and reach the observation point from

different directions. Finally, this amplitude is squared to obtain the overall spin-wave intensity $I_{SW}^{final}(\theta_{vg}, d)$ occurring at a distance d from the source and in the direction θ_{vg} in relation to the external magnetic field.

Spin-wave beams occur if the curve $I_{SW}^{final}(\theta_{vg}, d)$ exhibits pronounced peaks into certain directions θ_B. The angles θ_B of the theory curve shown in Figure 2b belong to the maxima of the calculated intensity distribution $I_{SW}^{final}(\theta_{vg})$ when assuming a distance of $d = 10\,\mu m$ and using the parameters of the investigated system (material parameters of CoFeB, $\mu_0 H_{ext} = 75$ mT, $w_{eff} = 1.3\,\mu m$, and $f \in [10.8, 15.4]$ GHz).

Supporting Information

Supporting Information is available from the Wiley Online Library or from the author.

Acknowledgements

Conflict of Interest

The authors declare no conflict of interest.

Keywords

[1] A. Khitun, *J. Appl. Phys.* **2012**, *111*, 054307.
[2] T. Fischer, M. Kewenig, D. A. Bozhko, A. A. Serga, I. I. Syvorotka, F. Ciubotaru, C. Adelmann, B. Hillebrands, A. V. Chumak, *Appl. Phys. Lett.* **2017**, *110*, 152401.
[3] K.-S. Lee, S.-K. Kim, *J. Appl. Phys.* **2008**, *104*, 053909.
[4] N. Sato, K. Sekiguchi, Y. Nozaki, *Appl. Phys. Express* **2013**, *6*, 063001.
[5] R. L. Freeman, *Fundamentals of Telecommunications*. Wiley-IEEE Press, Hoboken, NJ **2005**.
[6] F. Heussner, M. Nabinger, T. Fischer, T. Brächer, A. A. Serga, B. Hillebrands, P. Pirro, *Phys. Status Solidi RRL* **2018**, *12*, 1800409.
[7] Q. Wang, P. Pirro, R. Verba, A. Slavin, B. Hillebrands, A. V. Chumak, *Sci. Adv.* **2018**, *4*, e1701517.
[8] A. V. Sadovnikov, V. A. Gubanov, S. E. Sheshukova, Y. P. Sharaevskii, S. A. Nikitov, *Phys. Rev. Appl.* **2018**, *9*, 051002.
[9] V. E. Demidov, J. Jersch, S. O. Demokritov, K. Rott, P. Krzysteczko, G. Reiss, *Phys. Rev. B* **2009**, *79*, 054417.
[10] A. V. Chumak, V. I. Vasyuchka, A. A. Serga, B. Hillebrands, *Nat. Phys.* **2015**, *11*, 453.
[11] B. Lenk, H. Ulrichs, F. Garbs, M. Münzenberg, *Phys. Rep.* **2011**, *507*, 107.
[12] V. V. Kruglyak, S. O. Demokritov, D. Grundler, *J. Phys. D: Appl. Phys.* **2010**, *43*, 264001.
[13] A. Khitun, M. Bao, K. L. Wang, *J. Phys. D: Appl. Phys.* **2010**, *43*, 264005.
[14] G. Csaba, A. Papp, W. Porod, *J. Appl. Phys.* **2014**, *115*, 17C741.
[15] D. Sander, S. O. Valenzuela, D. Makarov, C. H. Marrows, E. E. Fullerton, P. Fischer, J. McCord, P. Vavassori, S. Mangin, P. Pirro, B. Hillebrands, A. D. Kent, T. Jungwirth, O. Gutfleisch, C. G. Kim, A. Berger, *J. Phys. D: Appl. Phys.* **2017**, *50*, 363001.
[16] C. Liu, J. Chen, T. Liu, F. Heimbach, H. Yu, Y. Xiao, J. Hu, M. Liu, H. Chang, T. Stueckler, S. Tu, Y. Zhang, Y. Zhang, P. Gao, Z. Liao, D. Yu, K. Xia, N. Lei, W. Zhao, M. Wu, *Nat. Commun.* **2018**, *9*, 738.
[17] P. Graczyk, M. Zelent, M. Krawczyk, *New J. Phys.* **2018**, *20*, 053021.
[18] M. Madami, S. Bonetti, G. Consolo, S. Tacchi, G. Carlotti, G. Gubbiotti, F. B. Mancoff, M. A. Yar, J. Åkerman, *Nat. Nanotechnol.* **2011**, *6*, 635.
[19] S. J. Hämäläinen, M. Madami, H. Qin, G. Gubbiotti, S. van Dijken, *Nat. Commun.* **2018**, *9*, 4853.
[20] V. Veerakumar, R. E. Camley, *Phys. Rev. B* **2006**, *74*, 214401.
[21] J. J. Bible, R. E. Camley, *Phys. Rev. B* **2017**, *95*, 224412.
[22] V. E. Demidov, S. O. Demokritov, D. Birt, B. O'Gorman, M. Tsoi, X. Li, *Phys. Rev. B* **2009**, *80*, 014429.
[23] F. Heussner, A. A. Serga, T. Brächer, B. Hillebrands, P. Pirro, *Appl. Phys. Lett.* **2017**, *111*, 122401.
[24] T. Schneider, A. A. Serga, A. V. Chumak, C. W. Sandweg, S. Trudel, S. Wolff, M. P. Kostylev, V. S. Tiberkevich, A. N. Slavin, B. Hillebrands, *Phys. Rev. Lett.* **2010**, *104*, 197203.
[25] T. Sebastian, T. Brächer, P. Pirro, A. A. Serga, B. Hillebrands, T. Kubota, H. Naganuma, M. Oogane, Y. Ando, *Phys. Rev. Lett.* **2013**, *110*, 067201.
[26] R. Gieniusz, H. Ulrichs, V. D. Bessonov, U. Guzowska, A. I. Stognii, A. Maziewski, *Appl. Phys. Lett.* **2013**, *102*, 102409.
[27] J.-V. Kim, R. L. Stamps, R. E. Camley, *Phys. Rev. Lett.* **2016**, *117*, 197204.
[28] G. Duerr, M. Madami, S. Neusser, S. Tacchi, G. Gubbiotti, G. Carlotti, D. Grundler, *Appl. Phys. Lett.* **2011**, *99*, 202502.
[29] S. Tacchi, G. Duerr, J. W. Klos, M. Madami, S. Neusser, G. Gubbiotti, G. Carlotti, M. Krawczyk, D. Grundler, *Phys. Rev. Lett.* **2012**, *109*, 137202.
[30] K. Wagner, A. Kákay, K. Schultheiss, A. Henschke, T. Sebastian, H. Schultheiss, *Nat. Nanotechnol.* **2016**, *11*, 432.
[31] The direction of the external magnetic field does not necessarily have to be inverted since the spin-wave dispersion relation of the studied system shows symmetry under magnetic field reversal.
[32] T. Sebastian, K. Schultheiss, B. Obry, B. Hillebrands, H. Schultheiss, *Front. Phys.* **2015**, *3*, 35.
[33] K. Vogt, F. Y. Fradin, J. E. Pearson, T. Sebastian, S. D. Bader, B. Hillebrands, A. Hoffmann, H. Schultheiss, *Nat. Commun.* **2014**, *5*, 3727.
[34] A. Vansteenkiste, J. Leliaert, M. Dvornik, M. Helsen, F. Garcia-Sanchez, B. Van Waeyenberge, *AIP Adv.* **2014**, *4*, 107133.
[35] G. Talmelli, F. Ciubotaru, K. Garello, X. Sun, M. Heyns, I. P. Radu, C. Adelmann, T. Devolder, *Phys. Rev. Appl.* **2018**, *10*, 044060.
[36] B. A. Kalinikos, A. N. Slavin, *J. Phys. C: Solid State Phys.* **1986**, *19*, 7013.
[37] T. Brächer, O. Boulle, G. Gaudin, P. Pirro, *Phys. Rev. B* **2017**, *95*, 064429.